Technical Note

Dissipation Effects of Coastal Vegetation on Nearshore Structures under Wave Runup Loading

Aikaterini P. Kyprioti, S.M.ASCE[1]; Alexandros A. Taflanidis, A.M.ASCE[2]; and Andrew B. Kennedy, M.ASCE[3]

Abstract: Inundation events caused by hurricanes or tsunamis pose a substantial risk to the integrity of coastal infrastructure; however, their impact on the built environment can be greatly altered by natural and anthropogenic obstacles or disturbances to the flow, such as vegetation or neighboring structures. This paper investigates the impact of coastal vegetation on shoreline structural vulnerability due to wave runup loading. Using numerical simulation data, the load (base shear) and momentum flux are computed as a function of vegetation characteristics (length and density) for different excitation intensities (wave heights) at the location of a shoreline structure. This information is then used to estimate structural fragility. Motivated by recent reconnaissance data from Hurricane Matthew in 2016, emphasis is placed on the out-of-plane failure of infill masonry walls. Extension to a different structural typology, that of a reinforced concrete frame, is also discussed. Comparisons between different vegetation characteristics and the bare-earth case demonstrate the wave dissipation and reduction of structural fragility (and therefore ultimately vulnerability) achieved when vegetation is present for the investigated case-study structures. **DOI: 10.1061/(ASCE)ST.1943-541X.0002902.**

Author keywords: Coastal vegetation; Wave dissipation; Wave runup loading; Coastal structure vulnerability; Out-of-plane failure; Global structural failure.

Introduction

Overland flow from inundation events (IEs) during tsunamis or hurricanes is a common phenomenon and is extremely destructive for coastal infrastructure. Natural and anthropogenic obstacles located between a structure and wave can play a significant role in reducing the impact of such events by modifying the hydrodynamics, leading to decreased loads on nearshore structures (Shuto 1987; Mazda et al. 1997). Qualitatively, the reduction of damage behind vegetation—at least when the vegetation is not uprooted, which would have created vulnerabilities due to potential debris impact—is entirely expected; quantitatively, predictions of damage reduction behind vegetation in the swash zone (alternating wet/dry due to IE runup) are challenging. Although much effort has been applied toward bare-earth (neighboring structures and vegetation removed) estimates of IE hydrodynamic loads on structures (Attary et al. 2016; Alam et al. 2017) and the dissipative effect of vegetation on wave forces is widely acknowledged (Anderson and Smith 2014; Vuik et al. 2016), the prediction of the effects of obstacles along the flow remains problematic with respect to the imposed loading on structures and subsequent risk assessment (fragility curve estimation). Similarly, loading standards (ASCE 2016) consider solely the bare-earth case.

The impact of obstacles between the shore and the structure can be significant, as shown in Fig. 1. Here, wave and surge inundation from Hurricane Matthew (in 2016) came across a wide beach in Côteaux, Haiti. One section of the beach was largely bare, with a few coconut palms, whereas the other had dense vegetation. School structures on the bare-earth section suffered extensive wall failures (failures extending also to adjacent frame elements), whereas similar buildings (constructed with the same material, having similar orientation, and located in the same elevation) behind the vegetation suffered no structural or foundation damage from the waves and surge (Kijewski-Correa et al. 2018). The damaged school building appears to have been destroyed by low-frequency wave runup, as has been observed in Typhoon Haiyan (Roeber and Bricker 2015) and in other locations in Haiti during Hurricane Matthew (Kijewski-Correa et al. 2018). Similar reduction in IE loading behind solid obstacles has also been observed in laboratory and field studies (Hatzikyriakou et al. 2015; Tomiczek et al. 2016), but the emphasis in this paper is placed on coastal vegetation (semipermeable obstacle), which does not affect the ecology and aesthetics of the shoreline as drastically as human-made structures, offering a low-cost potential solution that can be adopted by both developed and developing countries (Tanaka et al. 2007).

In this study, structural loads due to wave loading behind vegetation are estimated using recent numerical results (Alagan Chella et al. 2020); these loads are then used to estimate structural damage. Motivated by the example shown in Fig. 1, the out-of-plane failure of infill masonry walls are examined as the main case study, while an extension to global fragility of a reinforced concrete frame is also discussed.

Estimation of Structural Loads behind Vegetation

To evaluate the impact of the vegetation on structural vulnerability, numerical simulation results from a recent computational fluid dynamics (CFD) study (Alagan Chella et al. 2020) are utilized to quantify the loads on the structure as a function of the vegetation

[1]Graduate Researcher, Dept. of Civil and Environmental Engineering and Earth Sciences, Univ. of Notre Dame, 156 Fitzpatrick Hall, Notre Dame, IN 46556. Email: akypriot@nd.edu

[2]Professor, Dept. of Civil and Environmental Engineering and Earth Sciences, Univ. of Notre Dame, 156 Fitzpatrick Hall, Notre Dame, IN 46556 (corresponding author). ORCID: https://orcid.org/0000-0002-9784-7480. Email: a.taflanidis@nd.edu

[3]Professor, Dept. of Civil and Environmental Engineering and Earth Sciences, Univ. of Notre Dame, 156 Fitzpatrick Hall, Notre Dame, IN 46556. Email: andrew.kennedy@nd.edu

Note. This manuscript was submitted on September 27, 2019; approved on September 1, 2020; published online on December 16, 2020. Discussion period open until May 16, 2021; separate discussions must be submitted for individual papers. This technical note is part of the ***Journal of Structural Engineering***, © ASCE, ISSN 0733-9445.

Fig. 1. (a) Aerial view by unmaned aerial vehicle (UAV) of a structurally intact school building behind dense vegetation (after the necessary repairing process, this structure can be reused) and a destroyed building on the adjacent exposed section of a beach in Haiti after Hurricane Matthew (in 2016); and (b) close-up of the damaged building (collapsed and unable to be repaired), with the intact school unit shown in the background. (Available in Kijewski-Correa et al. 2017.)

characteristics. The study couples an OpenFOAM model with an IHFOAM module for mangrove–fluid interaction to estimate water surface elevation and momentum flux behind a semipermeable obstacle representing vegetation, for different incident wave and obstacle parameters. The vegetation is assumed to have no prior damage due to any previous inundation events, and a solitary wave of specific height is simulated reaching the shore. All geometric characteristics of the simulation are dependent on a characteristic length scale s as shown in Fig. 2(a); standard Froude scaling is then used to translate the simulation results to the structural scale desired for analysis. The characteristic length s in the problem formulation has been introduced simply to facilitate an easier scaling of the results.

In all simulations, an impermeable rigid square cylinder (representing a structure) is located behind a semipermeable obstacle, and the forces exerted on the structure are directly calculated from hydrodynamic pressures. Additional runs are performed with the semipermeable obstacle but without the cylinder using the same input wave conditions. Therefore, this numerical setup provides information for (1) intensity measures (IMs) commonly used to describe structural fragility against IEs (Attary et al. 2016; Park et al. 2017), such as the momentum flux or the inundation depth (from runs with no structure), and (2) the forces directly exerted on the structure itself. The first type allows the quantification of the vulnerability using fragility curves readily available in the literature, and the latter type allows the analytical estimation of damages through a comparison of the capacity against the demand for the base shear.

Computational results include four solitary wave heights $H/s = [0.26, 0.37, 0.49, 0.6]$, for one vegetation length $L/s = 2.00$ with nine different values as the damping of the semipermeable obstacle: $\alpha = [0, 0.5, 1.0, 2.0, 5.0, 20, 40, 80, 120]\,\mathrm{m}^{-1}$, with $\alpha = 0$ representing the bare-earth case (no vegetation). The different α values ultimately represent different plant species (Tanaka et al. 2007; Anderson et al. 2011); for example $\alpha = 1\,\mathrm{m}^{-1}$ can describe dense mangroves (*rhizophora*) (Massel et al. 1999), $\alpha = 3\,\mathrm{m}^{-1}$ can describe Australian pine (*c. equisetifolia*) (Forbes and Broadhead 2007), and $\alpha = 73\,\mathrm{m}^{-1}$ can describe marsh grass (*s. alterniflora*) (Morgan et al. 2005). Damping of the semipermeable obstacle is characterized using the damping coefficient αL adopted from Mendez and Losada (2004). This measure of dissipation depends on the macroproperties of the obstacle (Dalrymple et al. 1984), and for IE corresponding to breaking wave runup, it is given by (Alagan Chella et al. 2020):

$$\alpha L = DC_D NL \tag{1}$$

where D = diameter of vegetation stems; C_D = drag coefficient; and N = stem density per unit ground area. This analysis assumes properties at the long wave limit of the Mendez and Losada (2004) framework; uncertainties increase if wave periods fall outside this range.

The numerical results utilized herein correspond to peak horizontal loads on the structure. Because loads are only taken at discrete intervals, and because loads show scatter about their narrow peaks due to impact (Peregrine 2003), regression was performed over the data to obtain analytical representations of the peak loads for use in fragility analysis. The regression was performed for the logarithm of the quantities of interest to ensure that all load predictions remain positive. Dimensionless results for the momentum flux (*MF*) and the base shear per unit length F_B as a function of the wave height H/s and the vegetation damping aL are shown in Figs. 2(b and c). Herein, ρ represents the water density and g the gravitational acceleration. The coefficient of determination is $R^2 = 0.98$ for F_B and $R^2 = 0.93$ for *MF*, showing an overall good match. Fig. 3 shows the base shear per unit length for the four specific wave heights, along with its standard deviation σ based on the regression errors. It should be noted that these results are specific to the geometry considered, and other geometries and incident wave conditions may generate much different loading.

Fragility Quantification

Out-of-Plane Failure of Infill Masonry Walls

The first case study considers the out-of-plane failure of unreinforced masonry infill walls (like the ones in Fig. 1). The mean out-of-plane capacity in the form of base shear per unit length of such walls can be approximated using the results of Angel et al. (1994) as follows:

$$F_c = 2f_m t R_1 R_2 \lambda \tag{2}$$

where f_m = masonry compressive strength in the vertical direction; t = wall thickness; R_1 and R_2 = reduction factors for prior in-plane damage (taken as equal to 1 for in-plane undamaged masonry) and nonrigid bounding frames, respectively; and λ = coefficient that is dependent on the slenderness ratio of the infill wall. Parameter R_2 is given by

$$R_2 = 0.357 + 2.49 \cdot 10^{-14} EI \le 1.0 \tag{3}$$

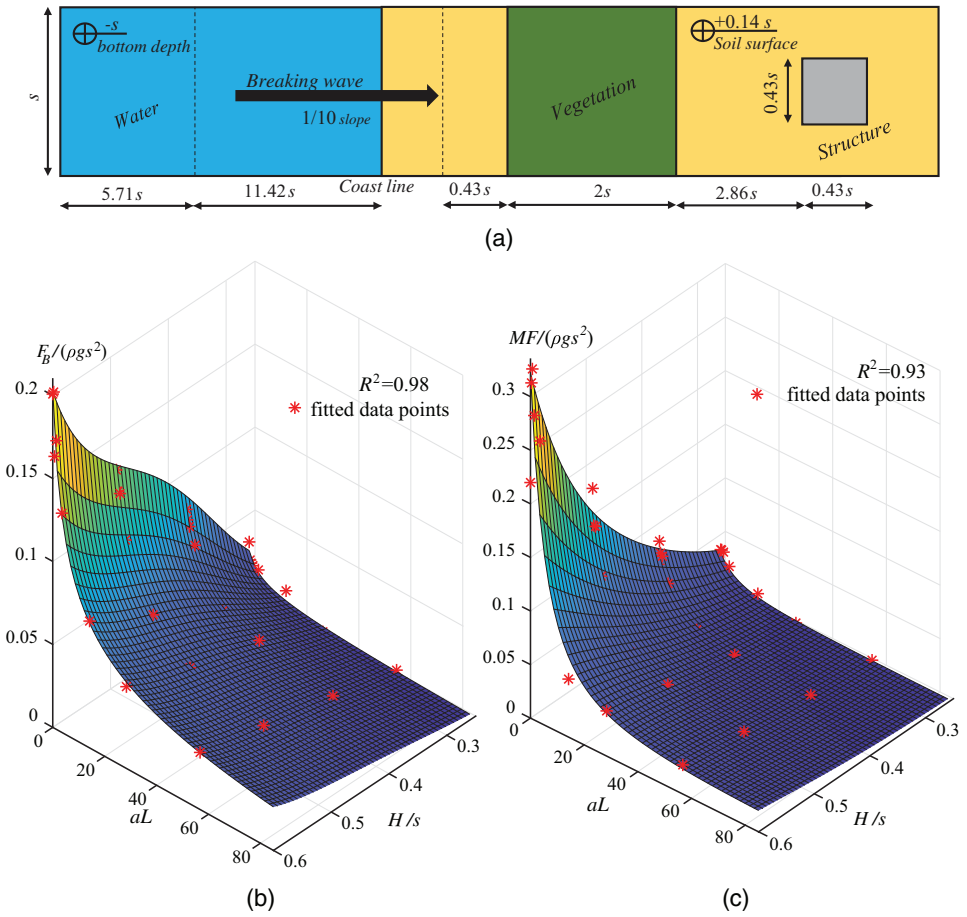

Fig. 2. (a) Geometry information for the numerical simulation setup used regarding the vegetation impact, with all dimensions proportional to the characteristic length scale factor s; and regression results for (b) the base shear per unit length at the structure F_B; and (c) the momentum flux MF in front of the structure as a function of the wave height H/s and the vegetation damping aL.

where EI = flexural stiffness of the smallest member of the confining frame at the panel edge with no continuity (in Nmm^2). For the λ estimation, the full height of the wall was used by Angel et al. (1994) with the assumption that loading was uniformly applied along the height. Because loading due to the IE extends only up to the water level, half of the total infill wall height is adopted here instead, to obtain an approximation for the slenderness ratio. This assumption is based on the fact that the wave heights in front of the structure did not typically surpass the midheight of the structure in the numerical simulations. Based on the recommendations of Komaraneni et al. (2011) for the masonry properties, a coefficient of variation of 30% is assumed for the out-of-plane capacity, following a lognormal distribution. It should be pointed out that any other capacity model, like the ones discussed by Ricci et al. (2018), could have been adopted here; the approximation based on Angel et al. (1994) was chosen due to its simplicity.

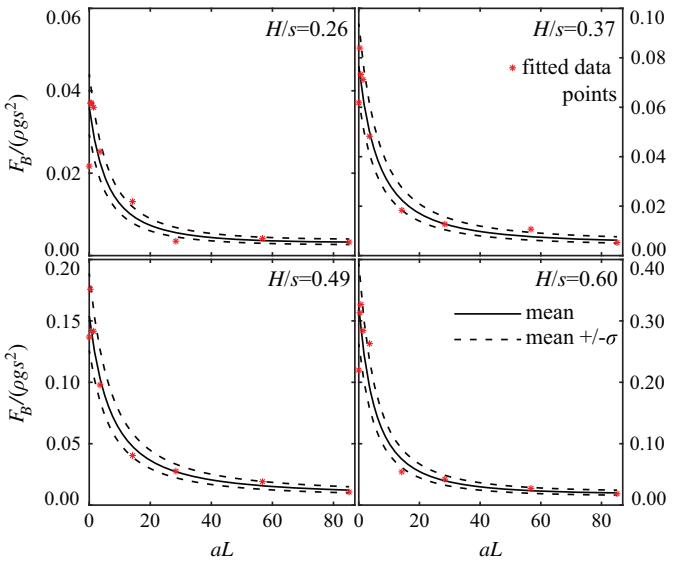

Fig. 3. Regression results for the base shear per unit length F_B for four different wave heights H/s.

The characteristic length for this configuration is selected as $s = 12$ m to resemble the case shown in Fig. 1. The geometric characteristics of the infill wall are chosen based on typical values encountered in Haiti: $l = 5$ m, $h = 2.80$ m, and $t = 0.15$ m for the length, height, and thickness, respectively. Concrete columns were assumed at both sides, having a square cross section of 0.15 m and a connecting beam with cross section 0.15×0.25 m. The material properties required for the concrete and infill masonry are $E_c = 20$ GPa and $f_m = 4.5$ MPa, respectively, according to Build Change (2011).

The probability of damage is estimated as:

$$P = \Phi\left[\frac{\ln(F/\beta)}{\sqrt{\sigma_r^2 + \sigma_b^2}}\right] \tag{4}$$

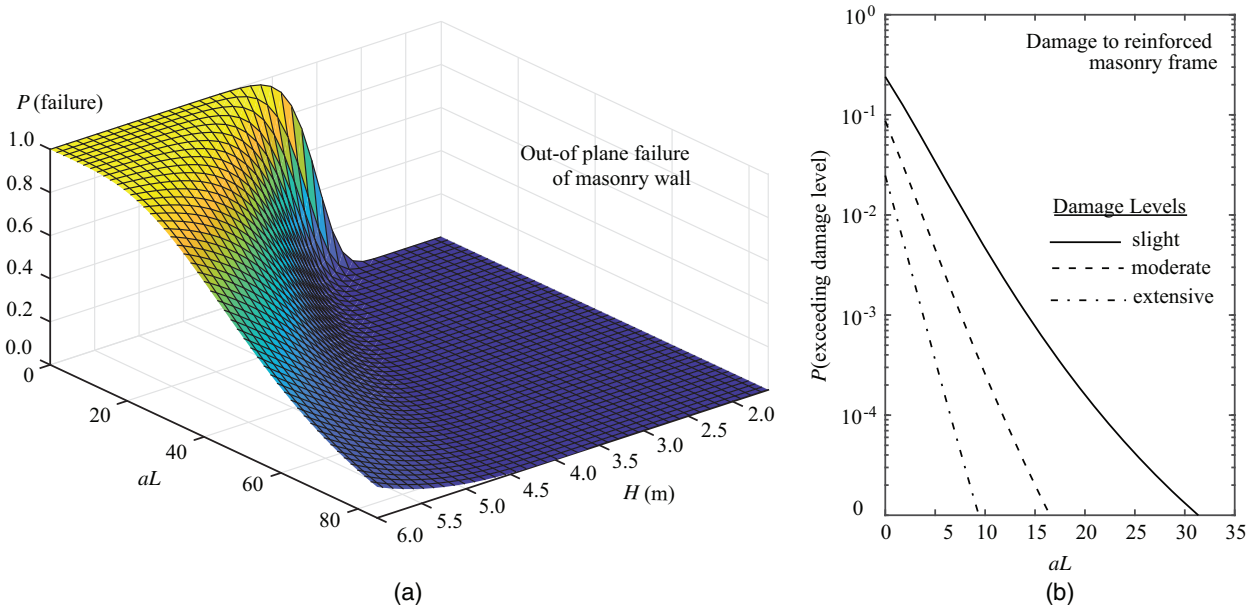

Fig. 4. (a) Probability of out-of-plane failure of a masonry wall as function of the breaking wave height H and the vegetation dissipation parameter αL; and (b) probability of exceedance for different damage states for the reinforced concrete frame as function of the vegetation dissipation parameter αL.

where F = demand (base shear per unit length) provided by the regression curve in Fig. 2(b); β = median capacity provided by Eq. (2); σ_r = root-mean squared error for the regression; and σ_b = coefficient of variation for the capacity. Results are presented in Fig. 4(a) as the probability of out-of-plane failure for the infill wall versus the density of the vegetation and the breaking wave height. As can be observed, increasing the density of the vegetation for a specific offshore wave height results in lower forces, decreasing significantly the probability of failure for the shielded structure. Looking along the different curves, the more energy the wave carries (higher offshore wave height), the more destructive it tends to be, although denser vegetation is able to dramatically reduce damages even in such instances.

Results show that for the bare-earth case, failure is likely ($P > 10\%$) for wave heights greater than 2.75 m. Although the exact wave heights at the site were not measured, this value seems very plausible based on the strength of Hurricane Matthew and the damages observed across the southern coast of Haiti (Kijewski-Correa et al. 2018). For the same wave height, and for $aL > 2.47$ (or $a > 0.103$ m^{-1}), the probability of failure becomes small (smaller than 1%), indicating complete protection by the vegetation. Even for an increased wave height of 4.0 m, failure probability becomes again smaller than 1% for $aL > 48$ (or $a > 2$ m^{-1}). These values of a are clearly much smaller than the vegetation front that protected the school building, which almost certainly had $aL > 100$, indicating that the results agree with the behavior observed in Fig. 1. It should be noted that the finite length of vegetation in Haiti compared with the longer lengths assumed in the simulations would likely contribute to an increase of the loads on the schools. Still, the agreement is very encouraging.

Global Failure for a Reinforced Concrete Frame Structure

To further showcase how the methodology can be extended to other typologies, the second case study considers the school building described in detail by Alam et al. (2017), having a lateral force–resisting system of RC moment-resisting frames in both longitudinal and transverse directions. The derived fragility curves from Alam et al. (2017) are directly used here. Specifically, the curves connecting momentum flux (IM) to probability of damage for different damage states (slight, moderate, and extensive) based on global failure criteria are utilized. The same characteristic length $s = 12$ m is used, and results are presented only for the largest breaking wave height $H/s = 0.6$, since other wave-height cases lead to insignificant effects on this structural typology.

The probability of exceeding each damage state is given by Eq. (4) where F is the momentum flux IM provided by the regression curve in Fig. 2(c), β and σ_b are the median and logarithmic standard deviation for each damage state fragility from Alam et al. (2017), and σ_r is the root-mean squared error for the IM regression. Results are reported in Fig. 4(b) as the probability of exceeding the different damage states. The results verify the trends observed in the previous case study: the vegetation provides significant dissipation and protection for the structure with probabilities for all damage states drastically decreasing.

Conclusions

In this paper, the effect of coastal vegetation on the vulnerability of offshore line structures during inundation events was investigated. Readily available literature data for simulation of breaking waves over vegetation was used to provide the necessary intensity measures or forces exerted on the structure. For two different structural typologies, this information was coupled with either fragility curves from the literature or analytical capacity predictions to estimate the probability of damage for different failure scenarios. Outcomes for these case-study examples showcase that the protection this vegetation can offer is substantial and can lead to a significant reduction in the vulnerability of the shielded structure. Results for the first example agreed with the behavior observed during Hurricane Matthew, also shown in Fig. 1 previously, which had provided the motivation of this study. The second example showcased how the numerical estimation of wave loading proposed by Alagan Chella et al. (2020) can promote a comprehensive

calculation of structural damages, explicitly accounting for the effect of semipermeable obstacles, simply by coupling resultant IMs with readily available fragility estimates in the literature.

Data Availability Statement

Some data used during the study were provided by a third party [fragility function details from Alam et al. (2017)]. Direct requests for these materials may be made to the provider as indicated in the Acknowledgments. Some other data generated or used during the study are available from the corresponding author by request (regression surfaces shown in Fig. 2). Remaining models and code used during the study appear in the published article.

Acknowledgments

This work was funded by the National Institute of Standards and Technology and by the National Science Foundation under Grant Nos. CMMI 17-09357 and CMMI-17-27662. This support is gratefully acknowledged. Any opinions, findings, and conclusions or recommendations expressed in this material are those of the authors and do not necessarily reflect the views of the funding agencies. Authors would also like to thank the authors of the paper by Alam et al. (2017) for providing the fragility curve data used in the second case study.

References

Alagan Chella, M., A. B. Kennedy, and J. J. Westerink. 2020. "Wave runup loading behind a semipermeable obstacle." *J. Waterway, Port, Coastal, Ocean Eng.* 146 (4): 04020014. https://doi.org/10.1061/(ASCE)WW.1943-5460.0000569.

Alam, M. S., A. R. Barbosa, M. H. Scott, D. T. Cox, and J. W. van de Lindt. 2017. "Development of physics-based tsunami fragility functions considering structural member failures." *J. Struct. Eng.* 144 (3): 04017221. https://doi.org/10.1061/(ASCE)ST.1943-541X.0001953.

Anderson, M. E., and J. M. Smith. 2014. "Wave attenuation by flexible, idealized salt marsh vegetation." *Coastal Eng.* 83 (Jan): 82–92. https://doi.org/10.1016/j.coastaleng.2013.10.004.

Anderson, M. E., J. M. Smith, and S. K. McKay. 2011. *Wave dissipation by vegetation*. Vicksburg, MS: US Army Engineer Research and Development Center Coastal and Hydraulics.

Angel, R., D. P. Abrams, D. Shapiro, J. Uzarski, and M. Webster. 1994. *Behavior of reinforced concrete frames with masonry infills*. Urbana, IL: Univ. of Illinois at Urbana–Champaign Engineering Experiment Station, College of Engineering.

ASCE. 2016. *Minimum design loads for buildings and other structures*. ASCE/SEI 7. Reston, VA: ASCE.

Attary, N., J. W. van de Lindt, V. U. Unnikrishnan, A. R. Barbosa, and D. T. Cox. 2016. "Methodology for development of physics-based tsunami fragilities." *J. Struct. Eng.* 143 (5): 04016223. https://doi.org/10.1061/(ASCE)ST.1943-541X.0001715.

Build Change. 2011. *Calculation report for confined masonry housing*. Denver: Build-Change Post-Earthquake Housing Reconstruction Technical Assistance Program.

Dalrymple, R. A., J. T. Kirby, and P. A. Hwang. 1984. "Wave diffraction due to areas of energy dissipation." *J. Waterway, Port, Coastal, Ocean Eng.* 110 (1): 67–79. https://doi.org/10.1061/(ASCE)0733-950X(1984)110:1(67).

Forbes, K., and J. Broadhead. 2007. *The role of coastal forests in the mitigation of tsunami impacts*. Bangkok, Thailand: Food and Agriculture Organization Regional Office for Asia and the Pacific.

Hatzikyriakou, A., N. Lin, J. Gong, S. Xian, X. Hu, and A. Kennedy. 2015. "Component-based vulnerability analysis for residential structures subjected to storm surge impact from Hurricane Sandy." *Nat. Hazards Rev.* 17 (1): 05015005. https://doi.org/10.1061/(ASCE)NH.1527-6996.0000205.

Kijewski-Correa, T. L., A. B. Kennedy, A. A. Taflanidis, and D. O. Prevatt. 2018. "Field reconnaissance and overview of the impact of Hurricane Matthew on Haiti's Tiburon Peninsula." *Nat. Hazards* 94 (2): 627–653. https://doi.org/10.1007/s11069-018-3410-0.

Kijewski-Correa, T. L., A. A. Taflanidis, A. B. Kennedy, A. Prevatt, and M. Kathleen. 2017. "RAPID: Multi-hazard performance of load bearing wall systems: A case study following the January 2010 Earthquake and October 2016 Hurricane Matthew." Accessed December 1, 2017. https://www.designsafe-ci.org/data/browser/public/designsafe.storage.published//PRJ-1763.

Komaraneni, S., D. C. Rai, and V. Singhal. 2011. "Seismic behavior of framed masonry panels with prior damage when subjected to out-of-plane loading." *Earthquake Spectra* 27 (4): 1077–1103. https://doi.org/10.1193/1.3651624.

Massel, S., K. Furukawa, and R. Brinkman. 1999. "Surface wave propagation in mangrove forests." *Fluid Dyn. Res.* 24 (4): 219. https://doi.org/10.1016/S0169-5983(98)00024-0.

Mazda, Y., M. Magi, M. Kogo, and P. N. Hong. 1997. "Mangroves as a coastal protection from waves in the Tong King delta, Vietnam." *Mangroves Salt Marshes* 1 (2): 127–135. https://doi.org/10.1023/A:1009928003700.

Mendez, F. J., and I. J. Losada. 2004. "An empirical model to estimate the propagation of random breaking and nonbreaking waves over vegetation fields." *Coastal Eng.* 51 (2): 103–118. https://doi.org/10.1016/j.coastaleng.2003.11.003.

Morgan, P. A., L. Curci, C. Dalton, and J. Miller. 2005. *Assessing the health of fringing salt marshes along the Fore River and its tributaries*. Armidale, Australia: Environmental Studies Faculty Publications, Univ. of New England.

Park, H., D. T. Cox, and A. R. Barbosa. 2017. "Comparison of inundation depth and momentum flux based fragilities for probabilistic tsunami damage assessment and uncertainty analysis." *Coastal Eng.* 122 (Apr): 10–26. https://doi.org/10.1016/j.coastaleng.2017.01.008.

Peregrine, D. 2003. "Water-wave impact on walls." *Annu. Rev. Fluid Mech.* 35 (1): 23–43. https://doi.org/10.1146/annurev.fluid.35.101101.161153.

Ricci, P., M. Di Domenico, and G. M. Verderame. 2018. "Empirical-based out-of-plane URM infill wall model accounting for the interaction with in-plane demand." *Earthquake Eng. Struct. Dyn.* 47 (3): 802–827. https://doi.org/10.1002/eqe.2992.

Roeber, V., and J. D. Bricker. 2015. "Destructive tsunami-like wave generated by surf beat over a coral reef during Typhoon Haiyan." *Nat. Commun.* 6 (1): 1–9. https://doi.org/10.1038/ncomms8854.

Shuto, N. 1987. "The effectiveness and limit of tsunami control forests." *Coastal Eng. Jpn.* 30 (1): 143–153. https://doi.org/10.1080/05785634.1987.11924470.

Tanaka, N., Y. Sasaki, M. Mowjood, K. Jinadasa, and S. Homchuen. 2007. "Coastal vegetation structures and their functions in tsunami protection: Experience of the recent Indian Ocean tsunami." *Landscape Ecol. Eng.* 3 (1): 33–45. https://doi.org/10.1007/s11355-006-0013-9.

Tomiczek, T., A. Prasetyo, N. Mori, T. Yasuda, and A. Kennedy. 2016. "Physical modelling of tsunami onshore propagation, peak pressures, and shielding effects in an urban building array." *Coastal Eng.* 117 (Nov): 97–112. https://doi.org/10.1016/j.coastaleng.2016.07.003.

Vuik, V., S. N. Jonkman, B. W. Borsje, and T. Suzuki. 2016. "Nature-based flood protection: The efficiency of vegetated foreshores for reducing wave loads on coastal dikes." *Coastal Eng.* 116 (Oct): 42–56. https://doi.org/10.1016/j.coastaleng.2016.06.001.